
Proceedings Paper:
Schwer, L. and Rigby, S.E. (2017) Reflected secondary shocks : some observations using afterburning. In: Proceedings of the 11th European LS-DYNA Conference. 11th European LS-DYNA Conference, 09-11 May 2017, Salzburg, Austria. DYNAmore GmbH . ISBN 9783981621549

Reflected Secondary Shocks: Some Observations using Afterburning

Len Schwer[1] and Samuel Rigby[2]

[1]Schwer Engineering & Consulting Services
[2]Department of Civil & Structural Engineering, University of Sheffield

1 Abstract

Afterburn models are typically used for charges in enclosed spaces to estimate quasi-static pressure. Also, any reflected shock that interacts with detonation products has the potential to add energy to the shock due to afterburning via additional gas mixing and heating.

Air blast tests that included normally reflected pressure measurements by the University of Sheffield, provided evidence of the so called 'secondary shock,' i.e. the recompression and expansion of the detonation products. This repeat test data provided an opportunity to explore calibration of the LS-DYNA afterburning model parameters to match the measured time of arrival and magnitude of the secondary shock. While the measured pressure histories alone are insufficient to uniquely calibrate the afterburn model, this manuscript attempts to illustrate the effect on the secondary shock of changing the four afterburn model parameters:

1. Start time for adding energy
2. End time for adding energy
3. Amount of energy to be added
4. Rate at which the energy is added, i.e. either linearly increasing or constant.

2 Introduction

Tyas et al. (2016) reported the results of a series of small scale open air tests using surface burst hemispherical PETN charges of 250 grams. Reflected pressures were measured at a rigid wall for charge standoffs of 2, 4 and 6 meters. The authors used a TNT equivalence of 1.5 for their PETN charge and then cited scaled ranges of 2.77, 5.55 and 8.32 m/kg$^{1/3}$, respectively. The goal of these tests was "assess the consistency of far-field blast waves from small PETN charges."

Included in the twice-repeated measured pressure wave forms, were the negative phases with their interruption by the so call 'secondary shock:'

> "Following detonation of an explosive material, a series of rarefaction expansion waves collapse inwards from the interface between the explosive and the surrounding air. These rarefaction waves coalesce at the centre of the explosive and reflect as a shock wave. Whilst these successive shocks are small in magnitude compared to the primary shock and are often ignored, the inward reflected shock immediately following the primary shock wave, typically referred to as the 'secondary shock', is a noticeable feature on blast pressure histories and usually arrives after the beginning of the negative phase." Rigby and Gitterman (2016)

The reflected pressures measured at a 2 meter standoff are shown in Figure 1 with an indication of the arrival, and magnitude, of the secondary shock at about 4.8ms. Similar data was reported for the 4 and 6 meter standoffs, but the focus of the present investigation will be the 2 meter standoff data.

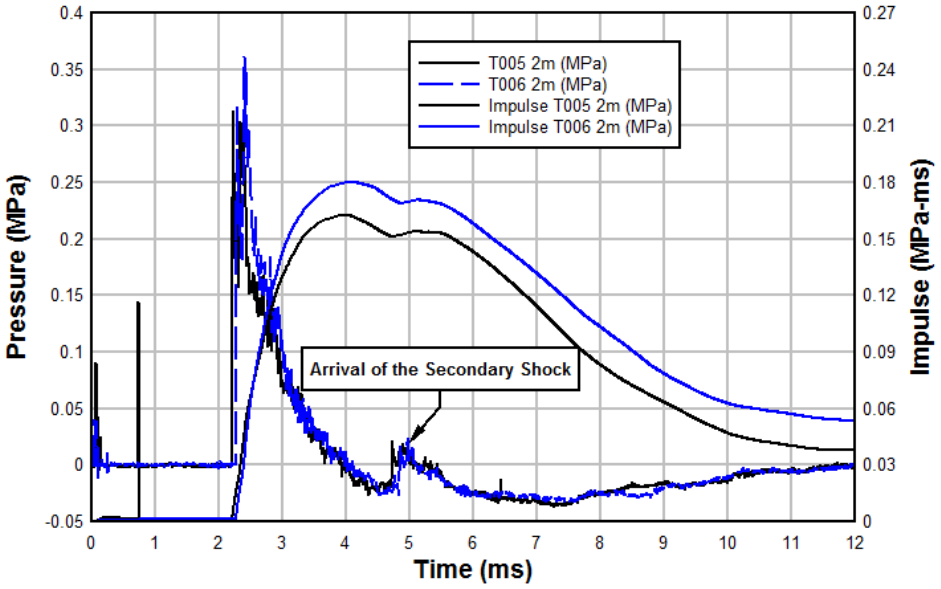

Figure 1 Repeated 2 meter standoff reflected pressure measurements for 250 gram hemispherical PETN charge.

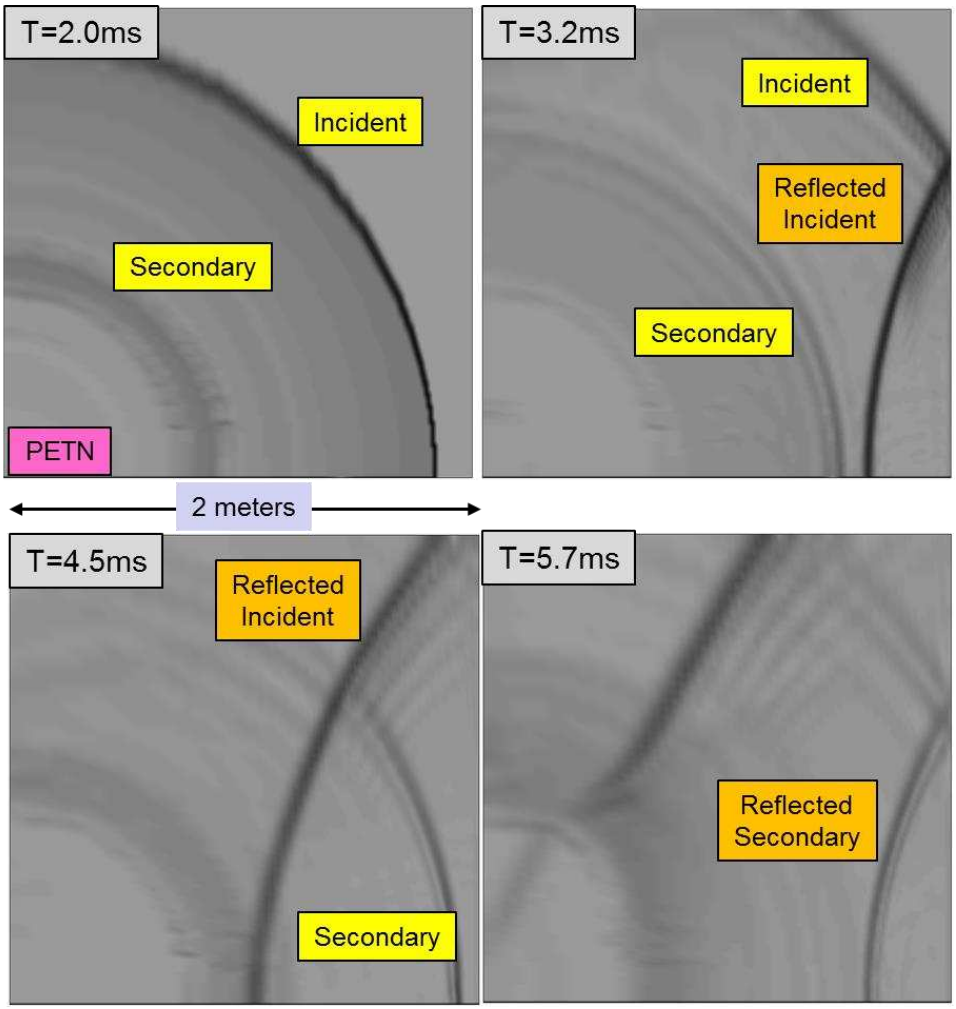

Figure 2 Numerical Schlieren images of the shocks and their approximate timing.

Figure 2 shows numerical Schlieren (density gradient) images from the present simulations to orient the reader to the shocks recorded in the Sheffield data. The incident shock is shown at 2ms propagates toward the rigid wall and is reflecting back toward the source at 3.2ms. At 4.5ms the reflected incident shock interacts with the rightward propagating secondary shock. The reflected secondary shock is shown at 5.7ms propagating back toward the source. Since the pressure gauge is at the rigid wall, only the reflected shocks are recorded, i.e. no incident shock is recorded.

3 Numerical Simulations

LS-DYNA Multi-Material Arbitrary Lagrange Eulerian (MM-ALE) simulation results are reported for 1D spherical, 2D cylindrical and 3D solid model. Although a 3D model is required to correctly model the experiments, much can be learned from the other two geometric approximations, especially the spherical model, via its increased mesh density and reduced CPU time.

3.1 Spherical Models

The 1D spherical model consisted of 10K beam elements each of length 0.2mm. Using a PETN[1] density of $1.77\times10^{-3}\mathrm{g/mm}^3$, the explosive charge occupied the left most beam region (origin) with a radius of 40.7mm representing a PETN charge mass of 500g, i.e. this spherical free air burst is equivalent to a 250g surface burst hemisphere. The right most end of the beam mesh had a prescribed zero velocity representing the rigid wall boundary.

Several tracer particles were placed along the beam, the most important located at $\mathrm{r}=1999\,\mathrm{mm}$, i.e. adjacent to the rigid wall boundary to capture the reflected pressure, another tracer particle at 1500mm served as a check on the incident pressure wave. Figure 3 compares the ConWep incident pressure at 1500mm for a 375g (1.5*250) TNT equivalent[2] hemispherical burst with the corresponding LS-DYNA 500g PETN incident pressure. The ConWep (TNT equivalent) incident pressure arrival is a little sooner (0.03ms) and has a 14% greater maximum pressure, than the LS-DYNA PETN incident pressure.

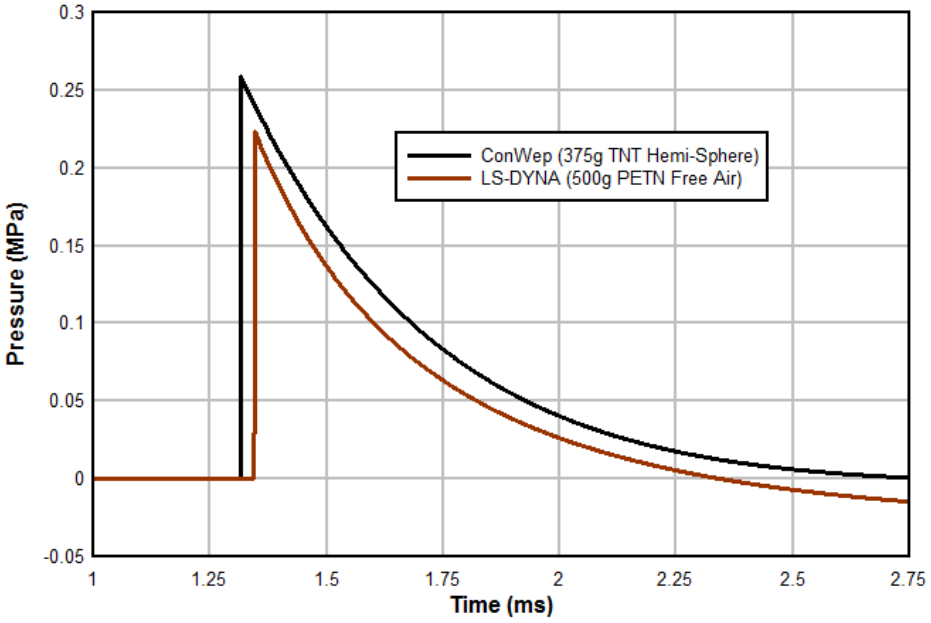

Figure 3 Comparison of ConWep and LS-DYNA incident pressures at 1500mm.

[1] The material characterizations for the PETN and air are included in an appendix.
[2] ConWep does not include a TNT equivalency for PETN.

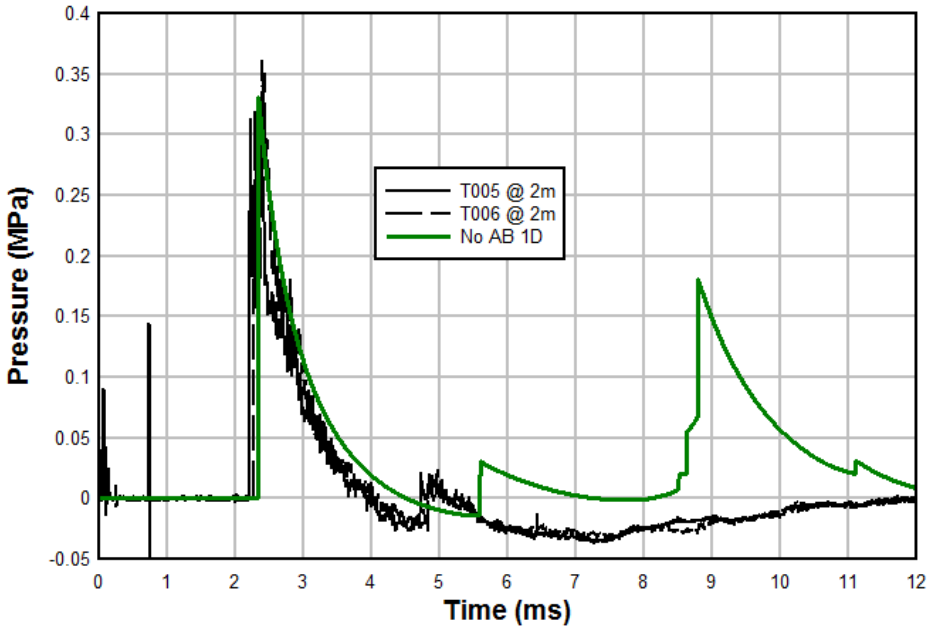

Figure 4 Comparison of reflect pressures for two repeat tests (T005 & T006) with LS-DYNA spherical simulation of the PETN charge without afterburning.

3.1.1 No Afterburn

Figure 4 compares the reflected pressure from two repeat Sheffield tests at 2m (T005 & T006) with the LS-DYNA spherical simulation without afterburning of the PETN. The two tests results are nearly identical and both indicate the arrival of the secondary shock at about 4.8ms which interrupts the negative phase with a pressure jump magnitude of 0.038MPa. The LS-DYNA reflected pressure has a similar reflected incident maximum pressure and time of arrival as the two test results, i.e. about 2.2ms and 3.3MPa. However, the simulated secondary shock arrives later at 5.5ms and has a pressure jump magnitude of about 0.045MPa also interrupting the negative phase. The remainder of the LS-DYNA pressure history is be attributed to the spherical geometry, as will be demonstrated in subsequent 3D models that more correctly represent the experimental setup.

3.1.2 Afterburning

The afterburning model extension of the LS-DYNA JWL EOS requires three additional inputs:

1. Amount of energy to be added,
2. Time period over which the energy is added,
3. Rate at which the energy is added, i.e. constant or linearly increasing.

Since this is an open air hemispherical charge detonation, a starting point is to assume complete afterburning. The various heat values for PETN from Chambers et al. (2002)[3] are provided in Table 1. The heat of combustion for PETN of 14.52GPa represents the detonation and complete afterburning. The energy available for afterburning is the combustion energy minus the detonation energy, and is the maximum additional energy to be added.

[3] The heat of detonation of 11.11GPa from Chambers et al. differs somewhat from the LLNL Explosives Handbook value of $E_0 = 10.1\text{GPa}$

Table 1: Table 1 Various heats for PETN with density $1.77\times10^{-3}\mathrm{g/mm^3}$

Heats	Energy/Mass (kJ/g)	Energy/Volume (GPa)
Formation	1.72	3.04
Detonation	1.50	11.11
Combustion	1.96	14.52
Afterburn	0.46	3.41

The initial assumption is of long duration afterburning event, starting shortly after detonation, 0.2ms, and lasting until the end of the secondary shock, i.e. the time when the negative pressure has returned to its value before the arrival of the secondary shock, say 6ms; see Figure 4. These are guesses to be refined via calibration of the afterburn model to the Sheffield data. The rate of afterburn additional energy was initially assumed to be linearly increasing; more on this parameter subsequently.

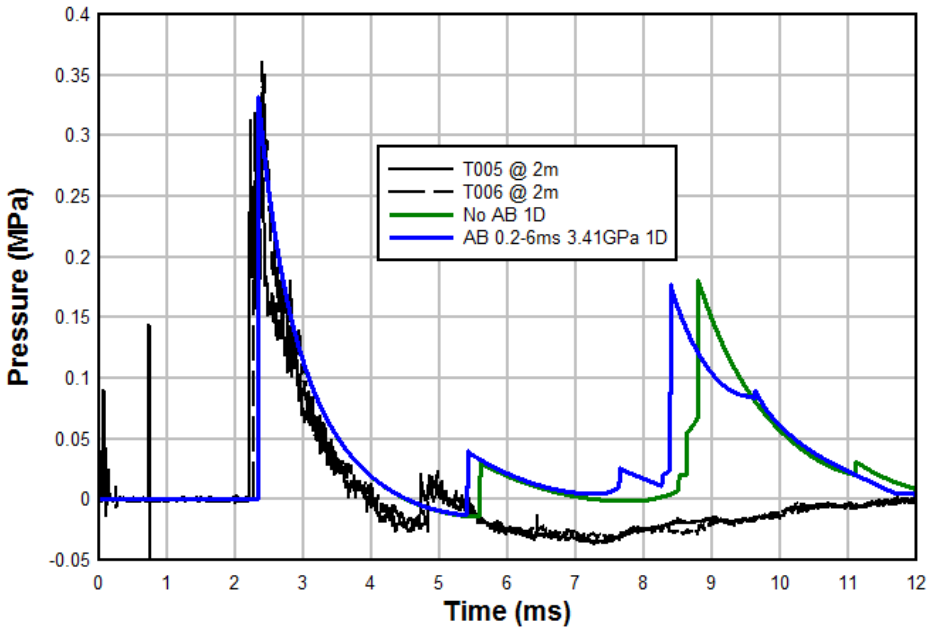

Figure 5 Sheffield data with comparison to LS-DYNA simulations without and with afterburning.

Figure 5 provides a comparison of the reflected pressure for the no afterburning with the corresponding full afterburning LS-DYNA result, and the experimental pressures histories as a referent. Inclusion of the PETN afterburning advances the arrival of the secondary shock by about 0.15ms and increases the pressure jump by about 0.009MPa (=0.051 – 0.042).

3.1.2.1 Afterburn Start Times

A parameter study was conducted varying the afterburn start times from 0, 0.2 and 0.5ms, keeping the same end time of 6ms and assuming full afterburning, i.e. $\mathrm{Q} = 3.41\mathrm{GPa}$. The results, shown in Figure 6, illustrates there was little sensitivity to these assumed afterburning start times.

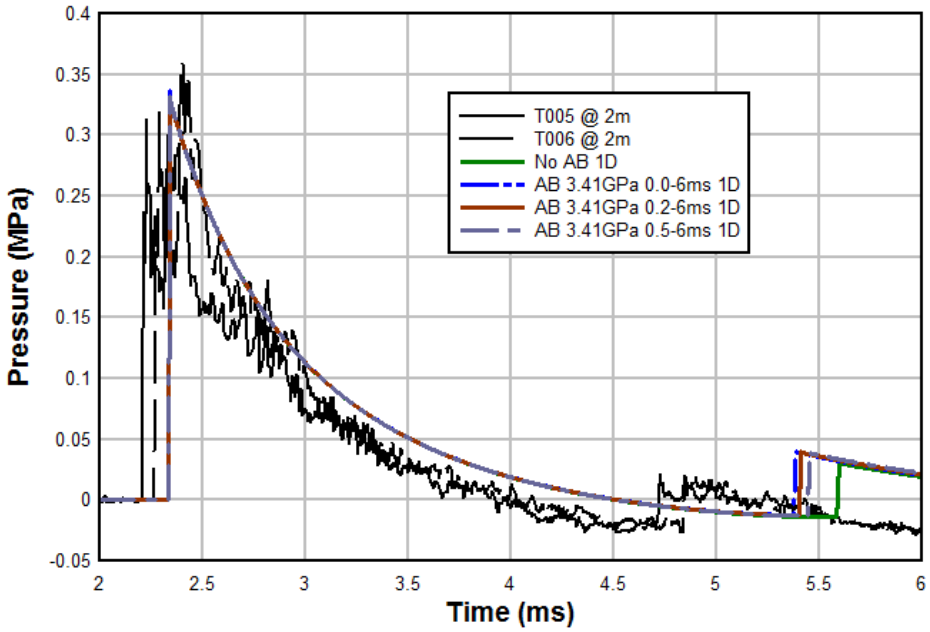

Figure 6 Comparison of pressure histories with varying afterburn start times: 0, 0.2, and 0.5ms.

3.1.2.2 Afterburn End Times

The next parameter study varied the afterburning end times of 2, 2.5, 3, 4, and 6ms, with a constant start time of 0.2ms and assuming full afterburning, i.e. $Q = 3.41\text{GPa}$. Figure 7 compares the reflected pressure from the five LS-DYNA end time afterburn parameter simulations. Decreasing the end time of the afterburn increases the arrival time of the secondary shock, and the magnitude of the pressure jump. The best time of arrival calibration with the Sheffield data occurs for an afterburn end time of 2.5ms.

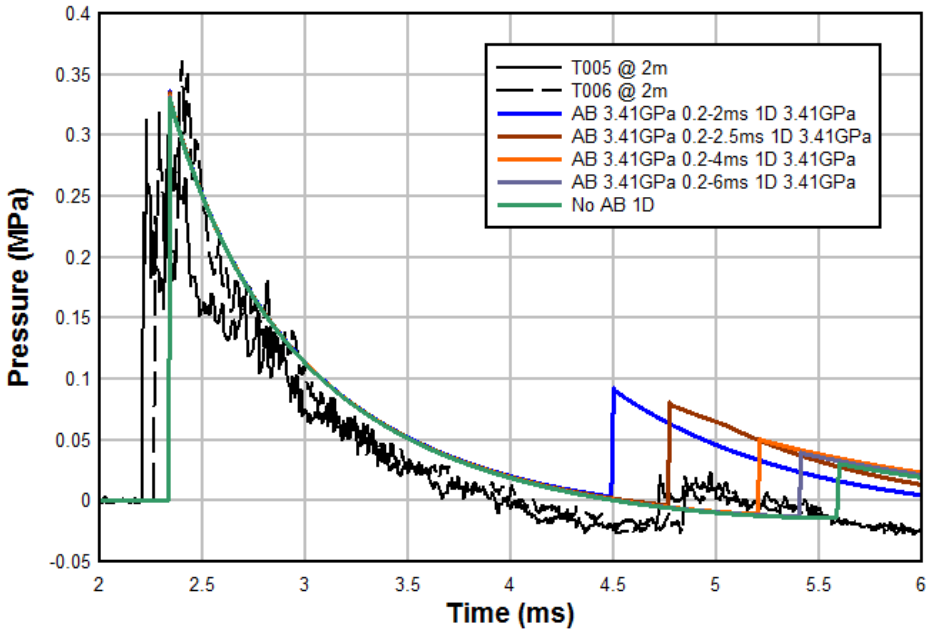

Figure 7 Results of afterburn end time parameter study with end times of 2.0, 2.5, 4.0 and 6.0ms.

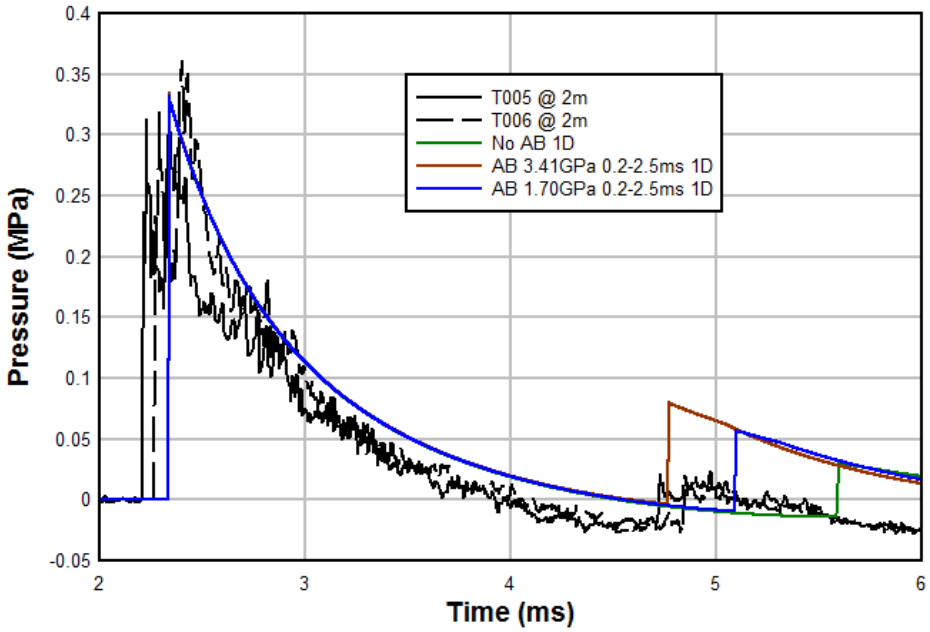

Figure 8 Results of amount of afterburn energy parameter study with start and end times of 0.2 and 2.5ms, respectively.

3.1.2.3 Afterburn Energy

The next afterburn parameter to be calibrated is the amount of afterburn energy to be added for the calibrated duration of 0.2 to 2.5ms. One parameter study was performed reducing the of afterburn energy by half, i.e. $Q = 1.7\text{GPa}$ representing incomplete afterburning. Figure 8 shows reducing the afterburn energy both delays the arrival of the secondary shock and decreases the secondary shock pressure jump.

3.1.2.4 Improving the Calibration

Reducing the end time of the afterburn causes the secondary shock to arrive earlier with an increased pressure jump and reducing the added energy causes the secondary shock to arrive later with a small pressure jump. Thus the possibility exists to vary both the afterburn end time and afterburn added energy to obtain a better calibration to the Sheffield data. Figure 9 shows an improved calibration after several adjustments of the afterburn end time and amount of added energy.

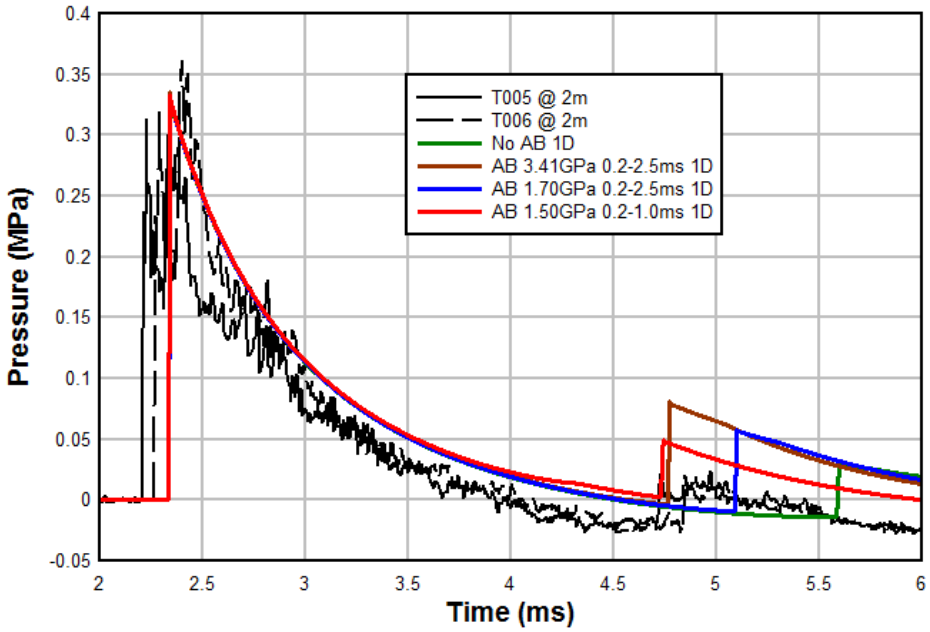

Figure 9 Improved calibration via changing both the afterburn end time and amount of added energy.

3.1.2.5 Afterburn Energy Addition Rate

The final afterburn option to be investigated in the LS-DYNA implementation is adding the afterburn energy at a constant rate (OPT=1), or at a lineally increasing rate (OPT=2), as was done for all the previous simulations. Figure 10 shows the constant afterburn energy addition causes the secondary shock to arrive only slightly sooner than when the afterburn energy is added at a linearly increasing rate.

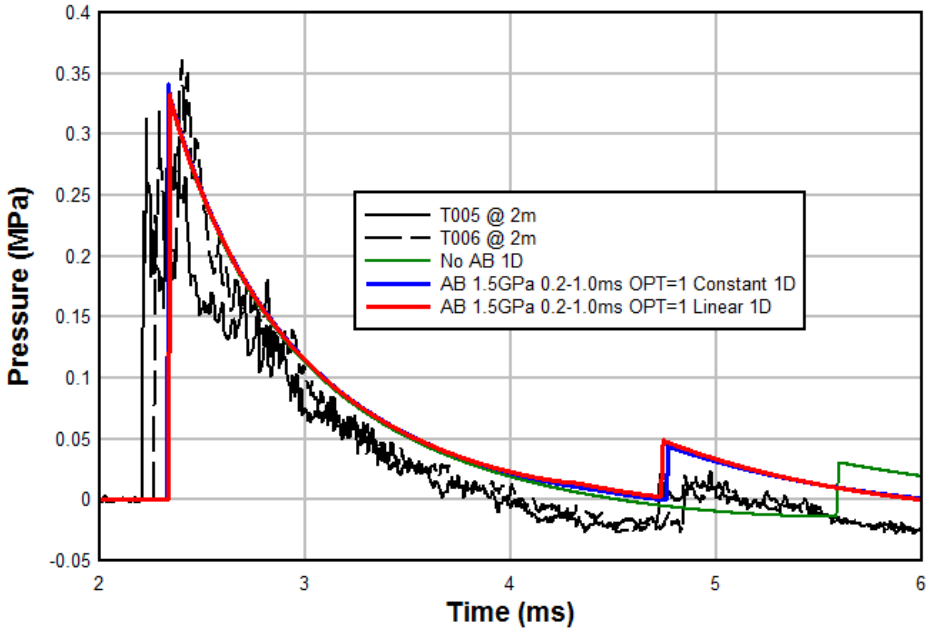

Figure 10 Reflected pressure comparison with afterburn energy added at a constant or linearly increasing rate.

3.2 Cylindrical Model

At this point it was decided to investigate how much the spherical geometry was contributing to the numerical results. Both 2D axisymmetric and 3D solid models were constructed both used the 1D spherical solution with a shortened duration of 2ms to initialize these multiple dimension models.

An Eulerian axisymmetric model was created with overall dimensions of 2x2m using a geometric ratio mesh with small elements at the bottom and right side (rigid wall), see Figure 11. The smallest elements were 5x5mm at the lower right corner and the largest were 51.4x51.4mm at the upper right corner, 10K elements in total. It should be noted that no mesh refinement was conducted at this point, as it was geometric effects that were the primary concern.

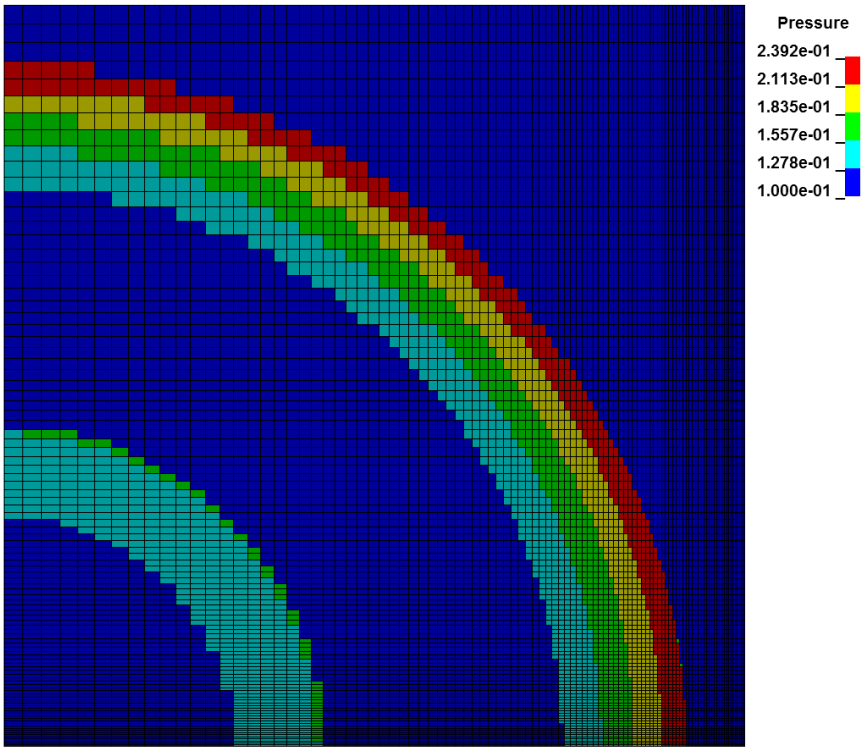

Figure 11 Axisymmetric model with pressure initialization at 2ms from the spherical model.

While mapping the 1D spherical solution at a time that places the pressure wave close to the rigid wall boundary is effective in minimizing axisymmetric mesh reflections over the period of interest, it does beg the question of how representative is the 1D spherical solution compared with a full 2D axisymmetric simulation. To address this question, an axisymmetric mesh, 2x2m, was constructed using uniform 5mm elements. Figure 12 compares the pressure histories for the mapped and no mapping simulations. The no map secondary shock arrived a little later, 0.14ms, than the mapped case, and has a slightly reduced secondary shock pressure jump. These differences are attributed to higher fidelity representation of the explosive in the 1D case, than in the 2D axisymmetric case, i.e. more than 200 elements across the charge radius in the 1D case, and only 8 elements in the 2D case.

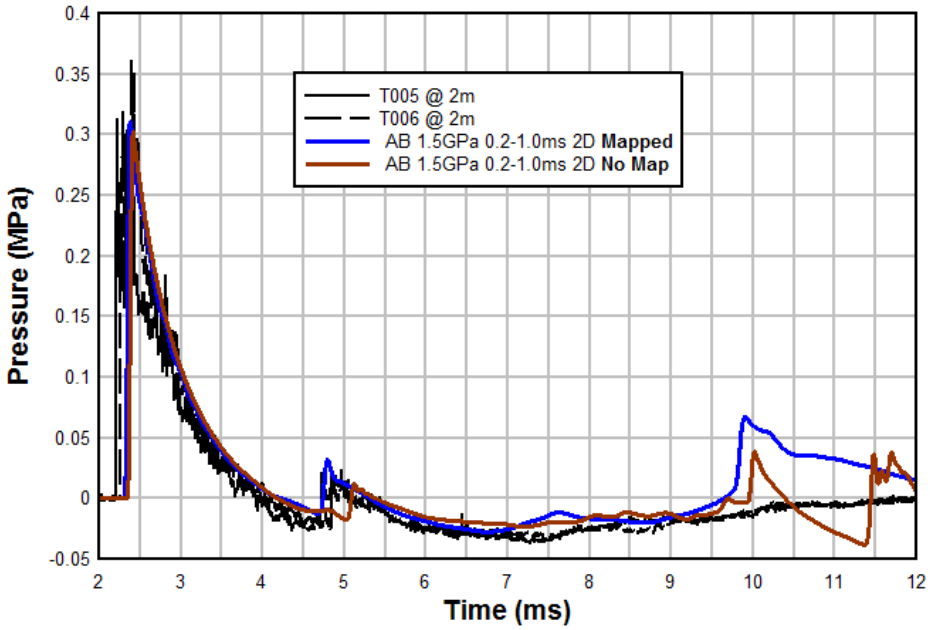

Figure 12 Comparison of mapped and no mapping axisymmetric (cylinder) pressure histories.

3.3 3D Model

An Eulerian 3D model was created with overall dimensions of 2x2x2m using a geometric ratio mesh with small elements at the bottom and right side (rigid wall), see Figure 13. As with the axisymmetric model, the smallest elements were again 5x5x5mm at the lower right corner nearest the pressure transducer and the largest were 51.4x51.4x51.4mm at the opposite corner, 10million elements in total. In both the axisymmetric and 3D models, a non-reflecting boundary was prescribed for the top surface of the mesh, all the other sides being either symmetry boundaries or the representation of the rigid wall in the experiments. Generally, non-reflecting boundaries are not recommended for blast problems as these boundaries are only appropriate for acoustic waves, i.e. pressure on the order of 0.2 atmospheres. A check on the total mass of the air indicated there was only a small amount of mass lost through advection across these boundaries.

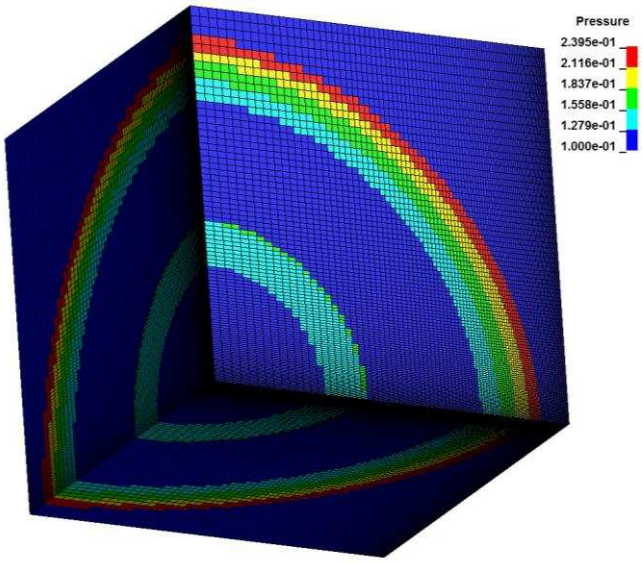

Figure 13 Three dimensional model with pressure initialization at 2ms from 1D spherical model.

3.4 Geometric Affects

Figure 14 compares the LS-DYNA afterburn reflected pressures from the 1D, 2D and 3D models; all simulations used an afterburn start time of 0.2ms and an end time of 1.0ms with added energy of $Q = 1.50\text{GPa}$. The axisymmetric and 3D models were initialized at 2ms with the results from the spherical simulation. It should also be recalled that the mesh refinement for the spherical case of 0.2mm is 25 times more refined than the smallest 5mm square axisymmetric and 3D elements.

The observations from the LS-DYNA comparisons shown in Figure 14 are:

1. While the arrival time of the secondary shock is the same in all geometric configurations, this due to the mapping of the spherical solution. Interestingly, the axisymmetric and 3D wave forms better track the Sheffield data's exponential decay up to the arrival of the secondary shock. The spherical results do not decay after the maximum pressure as rapidly[4].
2. The secondary shock pressure jump is slightly less for the axisymmetric and 3D simulations, both 0.045MPa, respectively, than for the spherical simulation (0.052MPa)
3. All three afterburn simulation results show a small tertiary shock arriving at about 7.5ms that is not indicated in the data.
4. The most dramatic difference is the 2D & 3D models exhibit a lack of large magnitude late time reflections that are evident in the spherical case starting at about 8.5ms. Note: there are reflections in the 2D results at about 9.7ms and in the 3D results at about 10ms, but both have a decreased magnitude relative to the previous lower order geometry approximation.

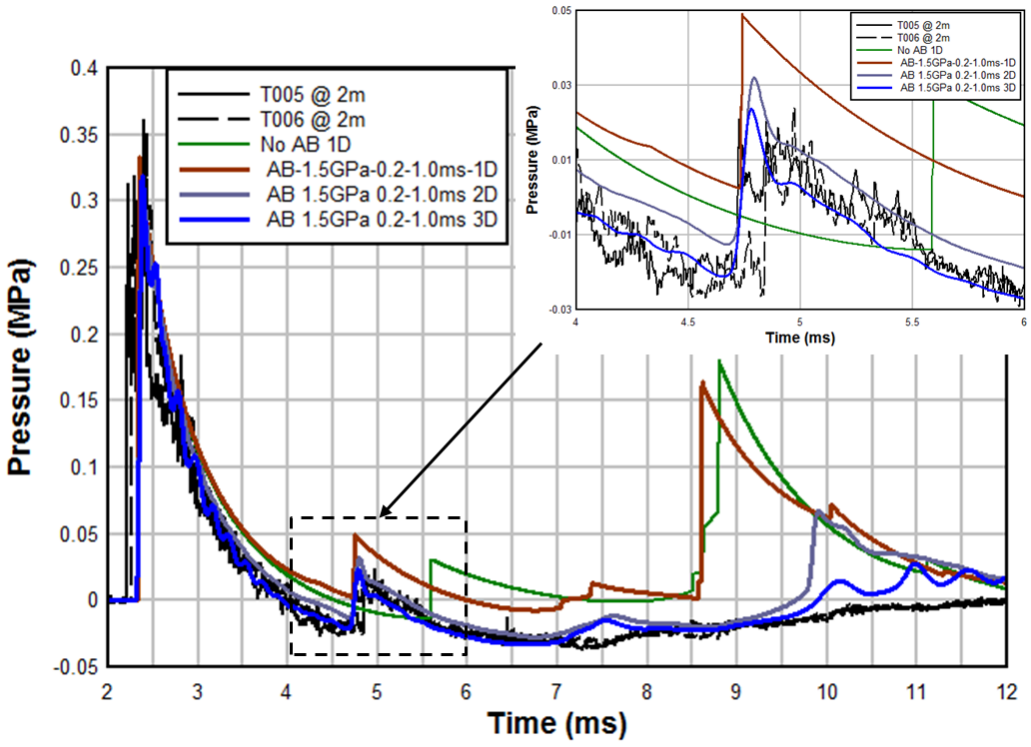

Figure 14 Comparison of spherical (1D), cylindrical (2D) and 3D modeling of reflected pressure with afterburning.

3.5 Multiple Secondary Shocks

As mentioned above, the simulation results indicate what appears to be more than one secondary shock. To possibly discriminate between secondary shocks and geometric mesh reflections, the no afterburn case was also run for the 3D mesh.

[4] There is a discussion in an Appendix on the role of artificial bulk viscosity on spherical results.

Figure 15 compares the 3D model reflected pressure histories with and without afterburning. The result with afterburning shows a small tertiary shock arriving at about 7.5ms that does not appear in the no afterburn result, or the Sheffield data. At about 8.6ms the no afterburn results indicate a small tertiary shock. The timing of the two tertiary shocks is approximately consistent with that of the two secondary shocks. At about 9.5ms the two numerical results are essentially coherent until they diverge again at about 10.5ms, likely from boundary reflections.

Although the Sheffield data does not clearly indicate a tertiary shock, there is a noticeable change in slope in the negative phase just before 8ms. Other experimenters have noted the existence of tertiary shocks in pressure measurements.

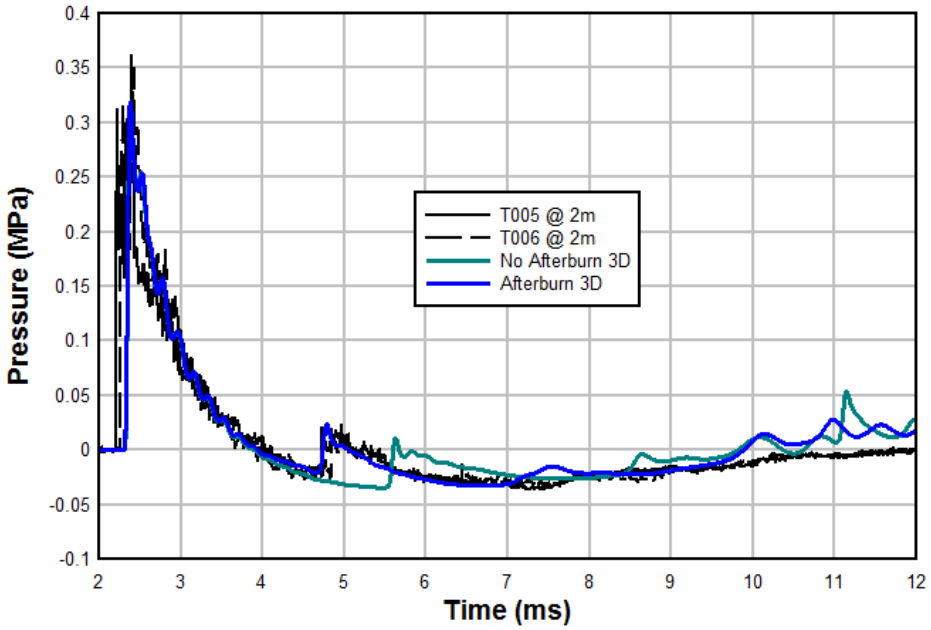

Figure 15 Comparison of reflected pressure histories from the 3D model with and without afterburn.

4 Summary

The inclusion of afterburning in a reflected pressure blast simulation was shown to affect the secondary shock arrival time and magnitude. There is not sufficient information available from measured pressure histories alone to uniquely calibrate the afterburn model parameters. An example of additional data that could be used to calibrate the start and end times would be temperature in the detonation products, as critical temperatures are required to maintain the afterburning chemical reaction.

The LS-DYNA implementation of afterburning requires four additional inputs to the standard JWL EOS:

1. Start time for adding energy
2. End time for adding energy
3. Amount of energy to be added
4. Rate at which the energy is added, i.e. either linearly increasing or constant.

Of these four parameters, the start time was found to have limited influence on the secondary shock response. The end time of the afterburning significantly affects the time of arrival of the secondary shock, i.e. decreasing the end time decreases the TOA. Similarly, the amount of afterburn energy added affects the time of arrival of the secondary shock, i.e. decreasing the added energy increases the TOA. The amount of afterburn energy added also affects the magnitude of the pressure jump that occurs due to the secondary shock. Thus iteratively changing both the end time and the amount of added energy allows for reasonable calibration to the Sheffield data. Finally, it was shown that using a constant or linearly increasing rate of afterburning did not significantly change the final calibrated result.

5 References

Tyas, A, J. Reay, S. Fay, S. Clarke, S. Rigby, J. Warren and D. Pope, (2016) “Experimental studies of the effect of rapid afterburn on shock development of near-field explosions,” International Journal of Protective Structures, Volume 7(3), pages 452–465.

Rigby S. and Y. Gitterman, (2016) “Secondary Shock Delay Measurements From Explosive Trials,” Military Aspects of Blast and Shock (MABS), Halifax, Nova Scotia, Canada, September 18-23.

Chambers, D.M., C.L. Brackett and O.D. Sparkman (2002) “Perspectives on Pentaerythritol Tetranitrate (PETN) Decomposition,” URCL-ID-148956
https://e-reports-ext.llnl.gov/pdf/244673.pdf

Noh, W.F. (1978) “Errors for Calculations of Strong Shocks Using an Artificial Viscosity and an Artificial Heat Flux,” Journal of Computational Physics, Volume 72, Pages 78-120.

6 Appendix – Material Characterizations

The units are grams-millimeters-milliseconds with the derived stress unit of MPa.

6.1 Air

```
$  Properties for Air
$
*MAT_NULL
$   MID   RO     PC   MU   TEROD  CEROD  YM  PR
    100, 1.29e-6, 0.0, 0.0, 0.0,   0.0
$
$========1=========2=========3=========4=========5=========6========
$                        EOS CARDS
$========1=========2=========3=========4=========5=========6========
$
$  Properties for Air
$
*EOS_Linear_Polynomial
$ EOSID  C0    C1   C2   C3   C4   C5  C6
$  100 , -0.1, 0.0, 0.0, 0.0, 0.4, 0.4, 0.0
   100 ,  0.0, 0.0, 0.0, 0.0, 0.4, 0.4, 0.0
$  e0    v0
  0.25, 1.0
```

6.2 PETN

```
$           Properties for PETN (1.77)  Dobratz 1981
$
*MAT_HIGH_EXPLOSIVE_BURN
$ MID    RO        D        PCJ    BETA
 2080, 1.77E-3,  8.30e3,   3.35E4,  0.0
$
$========1=========2=========3=========4=========5=========6========
$                        EOS CARDS
$========1=========2=========3=========4=========5=========6========
*EOS_JWL
```

```
$ EOSID     A        B       R1    R2    OMEG    E0      V0
 2080 ,  6.17E5, 16.926E3,  4.4,  1.20,  0.25,  10.1E3, 1.0
$
```

6.2.1 PETN with Afterburn

```
*MAT_HIGH_EXPLOSIVE_BURN
$ MID    RO         D        PCJ    BETA
 2180, 1.77E-3,  8.30e3,   3.35E4,  0.0
$
$========1=========2=========3=========4=========5=========6========
$                          EOS CARDS
$========1=========2=========3=========4=========5=========6========
$.....................................................................
$       Properties for PETN (1.77)  Dobratz 1981 & UCRL-JC-148956
$.....................................................................
*EOS_JWL_AFTERBURN
$ EOSID     A        B       R1    R2    OMEG    E0      V0
 2180 ,  6.17E5, 16.926E3,  4.4,  1.20,  0.25,  10.1E3, 1.0
$ OPT      QT        T1      T2
   2.0,  3.41E3     0.2,    2.5
```

7 Appendix – Artificial Bulk Viscosity with Spherical Simulations

Bill Noh (1978) showed that in a spherical geometry the standard form of artificial bulk viscosity introduces more numerical error than in axisymmetric and plane strain simulations. In particular, the time of arrival and maximum pressure can be calibrated to experimental data by adjusting the quadratic parameter Q_1 in the LS-DYNA implement of artificial bulk viscosity; the linear term provides damping of the pressure behind the shock. Figure 16 shows the change in time-of-arrival and maximum reflected pressure for various values of the quadratic artificial bulk viscosity parameter Q_1; note the LS-DYNA default value is $Q_1 = 1.5$.

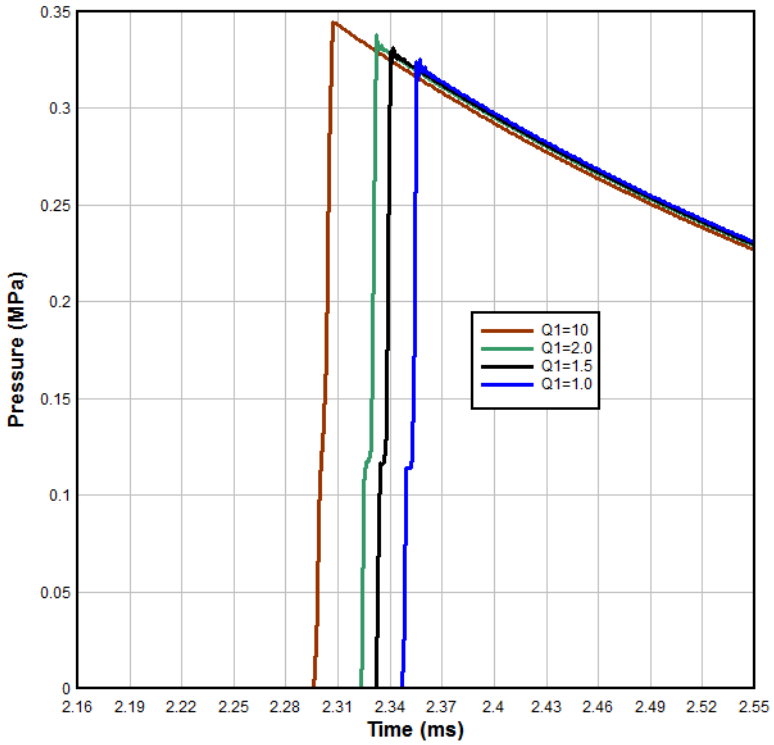

Figure 16 Effect of changing the artificial bulk viscosity Q_1 in a spherical blast wave simulation.